

# Early closed-loop results from the MMT's multi-laser guide star adaptive optics system

**Michael Lloyd-Hart, Christoph Baranec, N. Mark Milton, and Thomas Stalcup**  
*Center for Astronomical Adaptive Optics, The University of Arizona, Tucson, AZ 85721*

## ABSTRACT

Key advances in adaptive optics (AO) for both astronomical and military applications will be enabled through the deployment of multiple laser guide stars on large-aperture telescopes. Wider compensated fields of view than are now seen with conventional AO systems, even those equipped with single laser beacons, will be achieved with less field dependence of the delivered point-spread function. Correction to the diffraction limit over 1 arcmin fields with multi-conjugate AO and partial correction over 5 arcmin with ground-layer AO are anticipated. In this paper, we report preliminary closed-loop results from an adaptive optics system deploying multiple laser guide stars, operating at the 6.5 m MMT in Arizona, correcting the effect of the focus term from ground-layer turbulence. Five beacons are made by Rayleigh scattering of laser beams at 532 nm integrated over a range from 20 to 29 km by dynamic refocus of the telescope optics. The return light is analyzed by a unique Shack-Hartmann sensor that places all five beacons on a single detector, with electronic shuttering to implement the beacon range gate. The wavefront sensor divides the 6.5 m telescope pupil into 60 subapertures. Wavefront correction uses the telescope's unique deformable secondary mirror; significant image compensation will be realized at wavelengths of 1.2  $\mu\text{m}$  and longer. Global image motion, not sensed by the lasers, is measured from a natural star imaged onto a photon-counting CCD camera with a limiting magnitude for full speed corrections of  $V=17$ , with some correction remaining down to  $V=19$ .

## 1. INTRODUCTION

The current state of the art in adaptive optics (AO) is represented by high actuator count systems on large telescopes that deploy a single laser guide star (LGS). Such systems are now in use for both astronomical and military applications, but are fundamentally limited in their compensated field of view (FOV) because of tilt anisoplanatism and their degree of image correction because of focal anisoplanatism. Further advances in high resolution imaging may yet be made through the deployment of multiple laser guide stars (LGS) [1]. Constellations of beacons may be analyzed to yield a three-dimensional solution to the atmospherically induced wavefront aberration through tomography. Wider compensated fields of view than are now seen with conventional AO systems will be achieved with less field dependence of the delivered point-spread function (PSF). On telescopes of the current 8–10 m class, multi-conjugate AO (MCAO) using tomographic wavefront sensing is expected to yield correction to the diffraction limit in the near infrared over fields of 1 arcmin diameter. Compensation of low-lying turbulence by ground-layer AO (GLAO) is anticipated to give substantial improvement over natural seeing for larger fields up to 10 arcmin.

The promise of these new techniques, which are only now beginning to be explored at the telescope, is even greater for the next generation of extremely large telescopes (ELTs) [2,3]. Indeed, the primary motivation for our work at the 6.5 m MMT telescope described here is to understand how to design, build, and operate an AO system for the 25 m Giant Magellan Telescope (GMT), where multi-LGS tomographic wavefront sensing will be essential. Focal anisoplanatism, arising because rays of light from LGS at finite height sample the atmosphere differently from rays of starlight, is not so severe on 8 m telescopes as to prevent high Strehl imaging in the near infrared with a single LGS. But the error grows with aperture, and for ELTs the error would be prohibitive. It can be overcome however by combining signals from multiple LGS which collectively fill the volume of atmosphere perturbing the starlight.

The most straightforward of the multi-LGS techniques to implement, with important scientific application, is GLAO. By measuring and averaging the incoming wavefronts to a telescope at several different field points, an estimate of the common turbulence located near the entrance pupil of the telescope can be made, with the uncorrelated higher altitude contributions averaged away. This estimate, when applied to a deformable mirror conjugated near the telescope's pupil, can correct the atmospheric aberration close to the telescope which is common to all field points. It has been found empirically at various sites that typically half to two-thirds of the atmospheric turbulence lies in this ground layer [4–9], so when the technique is applied, the natural seeing will improve substantially over a large field. This will be of particular value to science programs that until now have not found any advantage in AO. Many observations that are normally carried out in the seeing limit will benefit from improved resolution and signal-to-noise, ultimately increasing scientific throughput. In this paper, we report early closed-loop results from a multi-LGS system operating in GLAO mode at the MMT.

## 2. THE MMT'S MULTI-LASER AO SYSTEM

For a full description of the multi-LGS and wavefront sensing systems, we refer the reader to previously published accounts [7,10]. Earlier work on laser-guided AO has been confined to a single beacon, usually created by resonance scattering in the sodium layer at 90 km altitude. For our work at the 6.5 m MMT, we have created five beacons generated by Rayleigh. Single Rayleigh beacons gated to an altitude of  $\sim 12$  km have previously been used for AO at small telescopes [11] but the strong focus anisoplanatism and incomplete sampling of higher turbulence make a single such beacon of little value for an 8 m class telescope.

The MMT's multiple laser guide star (LGS) AO system is comprised of four main components: the lasers and associated beam launch telescope, a Cassegrain mounted instrument containing the wavefront sensors (WFS), a real-time reconstructor computer and the adaptive secondary mirror (ASM) [12]. The beacons are generated with two doubled-YAG lasers at 532 nm, pulsed at 5 kHz, of 15 W each. The laser launch telescope combines the two beams in crossed polarizations, then breaks the combined beam into five that are projected from behind the secondary mirror of the MMT into a regular pentagon of beacons on the sky with a radius of 60 arcsec. These beacons are dynamically focused in the return optics [13] from an elevation of 20 to 29 km above the telescope. The long range gate, which greatly exceeds the telescope's normal depth of field at that range, increases the photon return and allows the use of low-power lasers.

The wavefront sensing instrument, built on a custom optical breadboard, is shown in Fig. 1. After wavefront compensation at the MMT's secondary mirror, light passes through a hole in the center of the breadboard to the entrance window of the science camera. This is a dichroic beam splitter which transmits light longward of  $1 \mu\text{m}$  into the science dewar and reflects visible light back up into the WFS. Laser light is separated by a notch reflector centered at 532 nm into the dynamic refocus optics and on to the LGS WFS. The remaining visible light from stars in the field, longward and shortward of 532 nm, is transmitted by the notch reflector to a fast tip-tilt camera with a searchable 2 arcmin field using an electron multiplying L3 CCD, a standard natural guide star (NGS) Shack-Hartmann WFS with  $12 \times 12$  subapertures which can be used for open-loop testing or other calibrations, and a wide field video camera used for acquisition.

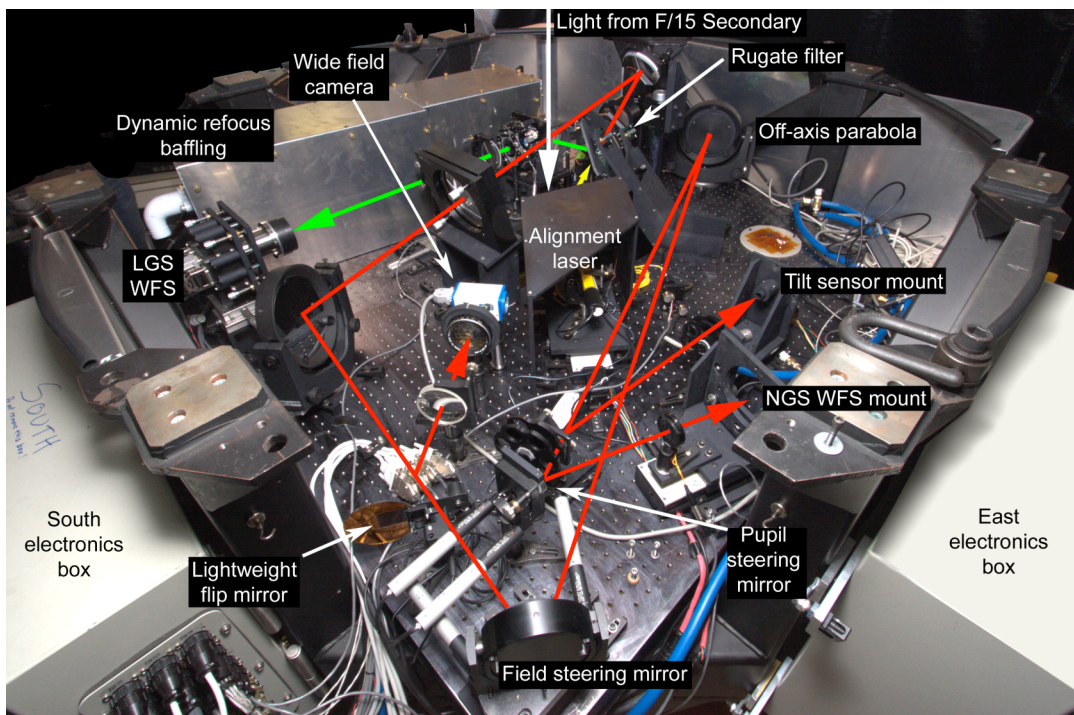


Fig. 1. Photograph of the wavefront sensing instrument. The main white arrow shows the light coming from the f/15 adaptive secondary. The yellow arrow shows visible light reflected off the tilted science instrument entrance window. The green arrow shows the path of the LGS light reflected off the rugate filter into the laser wavefront sensor. The red arrow shows the remaining visible light as it passes to the tilt, wavefront sensor and wide field cameras.

The images from all five laser beacons are recorded on a novel implementation of the Shack-Hartmann WFS, which includes the dynamic focus optics and a single electronically shuttered CCD. A prism array divides the pupil into 60 subapertures arranged in a hexapolar geometry as shown in Fig. 2. The LGS WFS may be run at frame rates up to 500 Hz with good signal-to-noise ratio.

The real-time reconstructor computer reads frames from the laser WFS and tilt sensor and computes corrections to be applied to the ASM. The hardware is a PC comprising a dual quad core Xeon X5355 CPU running at 2.66 GHz, with 2 GB of memory. It runs the CentOS operating system with RTAI real-time extensions, and uses an EDT PCI-DV framer grabber card for communication with the laser WFS controller. The software is written in C and has been developed in-house. In GLAO mode, the slopes from corresponding subapertures are averaged over all five beacons before being multiplied by the reconstructor matrix. In future use for LTAO, the reconstructor matrix will be five times larger which will require that the matrix multiplication software be parallelized and split across several CPUs.

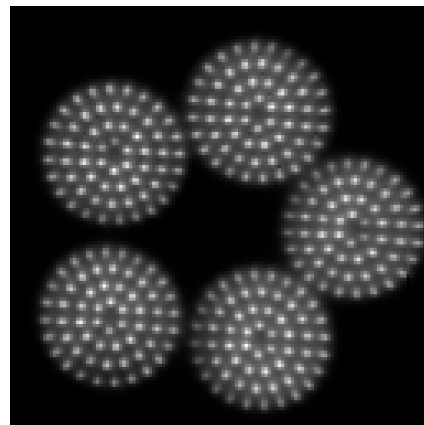


Fig. 2. Example frame from the MMT's laser WFS showing the five beacons sampling the pupil with 60 subapertures each. The range gate of the WFS camera is 20 to 29 km.

### 3. IMPACT OF GLAO

Ground-layer correction was first suggested by Rigaut [14] as a way to improve wide field imaging for large telescopes. Since then, numerous simulations have shown that GLAO can effectively and consistently improve the atmospheric seeing [4,15,16]. GLAO was first demonstrated using three bright natural guide stars on a 1.5 arcmin diameter with the Multi-conjugate Adaptive Optics Demonstrator (MAD) fielded at the VLT in early 2007 [17]. Because of the limited number of suitably bright natural guide star constellations on the sky, MAD was not designed to support routine science observations. However, plans are currently underway to implement GLAO at several telescopes around the world with a variety of techniques [18–22].

The MMT multiple laser AO system, after being in development for several years, is currently being commissioned. Its main goals are to prove the concepts of GLAO with LGS and laser assisted tomographic adaptive optics (LTAO), and to support science observations. In that capacity, beginning in early 2008, GLAO will provide diffraction-limited imaging in the thermal infrared bands from 3.5 to 10  $\mu\text{m}$  and substantial seeing improvement in K ( $\lambda = 2.2 \mu\text{m}$ ) and shorter bands over all the sky accessible above  $45^\circ$  elevation. With the addition of LTAO, anticipated in the summer of 2008, diffraction-limited operation will be extended down to H band (1.6  $\mu\text{m}$ ). The system's on-sky performance will allow GLAO and LTAO performance projections for the twin 8.4 m Large Binocular Telescope (LBT) [22], the 25 m GMT, and other ELTs.

Previous open-loop experiments have been carried out with the multi-LGS system at the MMT [23]. Wavefront data were recorded simultaneously from all five beacons and a natural star enclosed within the LGS constellation with the two Shack-Hartmann sensors synchronized. The average signal from the beacons was taken as a measure of the ground layer aberration. The difference between the average laser wavefront and the stellar wavefront is a measure of the degree of correction to be expected in closed loop. Fig. 3 shows sample PSFs computed from these residual wavefronts, with high-order aberrations added to model the uncorrected modes of the system, and servo lag of 0.02 s. A summary of PSF metrics by waveband is given in Table 1, including the full width at half maximum (FWHM) and  $\theta_{50}$  and  $\theta_{80}$ , the radii enclosing respectively 50% and 80% of the energy. The data were recorded in good seeing, and illustrate that in such conditions resolution better than 0.2 arcsec in H and K bands can be expected. Data recorded during periods of poor seeing bear out the result seen in previous work [4] that GLAO continues to perform well, delivering image resolution of 0.2 arcsec even in seeing at approximately the 80<sup>th</sup> percentile for the site.

### 4. OPERATION OF THE CLOSED-LOOP SYSTEM

The RLGS WFS is unusual in that the null points of the Shack-Hartmann spots are not centered on pixel boundaries. Furthermore, because it is not the aim of the closed-loop servo to correct all the wavefront error in each beacon, the spots are not always driven to these null points. It is therefore important that the RLGS WFS response be accurately

Table 1. Key figures of merit for PSFs corrected by GLAO in H and K bands. The values are based on simultaneous open-loop LGS and NGS wavefront measurements recorded at the MMT, and include the effects of uncorrected high-order aberration and servo delay that would pertain in a closed-loop AO system.

Metric	Field angle (arcsec)						Diffraction limit		Seeing limit	
	5		25		50					
	H	K	H	K	H	K	H	K	H	K
FWHM (arcsec)	0.10	0.10	0.13	0.12	0.14	0.13	0.052	0.070	0.36	0.34
$\theta_{50}$ (arcsec)	0.21	0.13	0.21	0.14	0.21	0.14	0.048	0.064	0.27	0.25
$\theta_{80}$ (arcsec)	0.51	0.46	0.51	0.47	0.51	0.47	0.13	0.13	0.52	0.51
Peak intensity	0.082	0.21	0.056	0.16	0.055	0.14	1.0	1.0	0.015	0.028

calibrated. The first step is the alignment of the telescope and science camera. The adaptive secondary mirror is set to the so-called ‘flat’ position: in fact, the non-aberrated aspheric shape expected of a rigid secondary mirror, determined from off-telescope calibrations. The telescope is then collimated, using feedback from the science camera looking at defocused starlight.

To calibrate the RLGS WFS, a bright star is placed on the NGS WFS and the loop is closed with this system. This reduces most of the effect of the atmosphere and provides a less aberrated path between the laser beacons and the laser WFS. While the NGS loop is closed, images of the laser beacons are recorded on the laser WFS over a period of a minute. The images are averaged and the centroid position of each Shack-Hartmann spot is calculated. These are used as the null points for the spots. This can be done without the NGS WFS, using just the flat position of the mirror, but more of the non-common path errors will be taken out if the closed-loop NGS system is used in the calibration. A  $6 \times 6$  pixel subaperture is defined around each spot on the RLGS WFS camera. The slopes within these subapertures are calculated from the averaged laser WFS frame and are saved as slope offsets along with the subaperture locations. A sky background frame is also taken by the reconstructor with the laser beacons turned off.

The system is then ready for closed-loop operation. Frames from the RLGS WFS are sent to the reconstructor. After background subtraction, spot positions are calculated for each subaperture by a correlation tracker algorithm and the offsets removed. The resulting vector of slopes is augmented by the latest global tip-tilt signals available from the tilt camera which runs asynchronously. Command updates for the adaptive secondary are generated by multiplying the augmented slope vector by the reconstructor matrix, and applying a scalar system gain. Before being sent to the mirror, the command vector is corrected for the presence of uncontrolled modes. In typical GLAO operation, 54 modes will be controlled, but the ASM has 336 actuators; including piston, there are therefore a total of 282 uncontrolled modes which may be excited by external perturbations such as wind buffet, vibration, or actuator cross-talk. To remove them from the mirror shape, the vector of capacitive sensor signals from all 336 actuators is multiplied by a modal filter matrix which spans the null space of the reconstructor matrix. The resulting vector is subtracted from the actuator command update vector on each cycle of the servo loop.

## 5. CLOSED-LOOP RESULTS

The first closed-loop result was obtained during a telescope run in July of 2007 of 4 nights. The run was almost entirely lost to weather, with only four hours of usable time during which the seeing was never better than 1.5 arcsec at 500 nm. This unfortunately limits the results we are able to show here. As a first test, a reconstructor matrix was

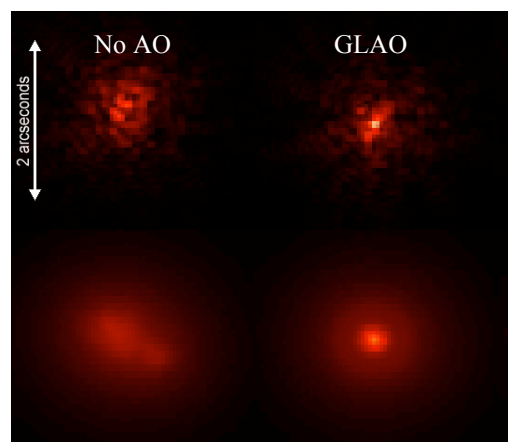


Fig. 3. Top: instantaneous PSFs with no correction (left) and GLAO correction (right). Bottom: simulated 60 s integrations with the same degrees of compensation.

built that controlled just global image motion from the NGS and focus from the average RLGS signal. The modal filter matrix accordingly removed all other modes from the command signal. Telemetry was recorded on the reconstructor; the seeing conditions at the time of the observations, calculated from the uncorrected laser modes were consistent with  $r_0(500\text{ nm}) = 8.1\text{ cm}$ , the 88th percentile for the telescope.

After calibration of the laser WFS, the hexapod holding the ASM was moved  $20\text{ }\mu\text{m}$  towards the primary mirror. This added a static focus offset of  $-426\text{ nm}$  for the AO system to correct in addition to the atmospheric term. Fig. 4 shows the measured residual focus and uncorrected  $45^\circ$  astigmatism modes as recovered from the recorded slope information from a single data set lasting 2 minutes on the laser wavefront sensor. The data were recorded with the system running at  $208\text{ Hz}$  update rate. The control loop gain was initially set to zero, raised to  $0.2$  at  $12.5\text{ s}$  and incrementally increased to  $0.9$ . As can be seen in figure 3, the measured focus mode moves towards a mean value of  $0\text{ nm}$  when the loop gain is increased from zero, correcting the static offset added with the movement of the hexapod.

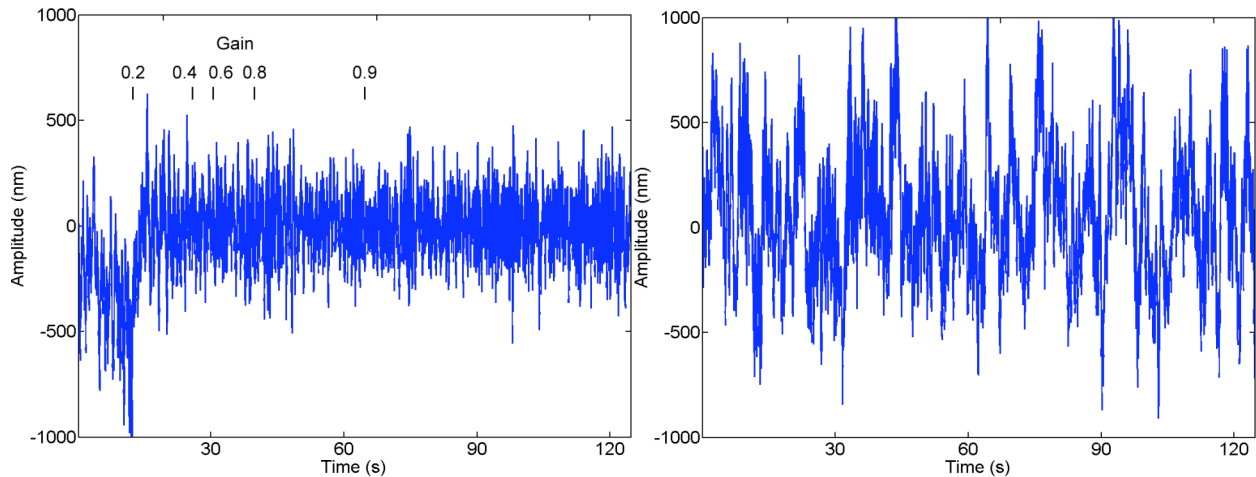


Fig. 4. (Left) Measured ground-layer focus mode during closed-loop correction of focus. The tick marks show when the gain factor, which starts at zero at time = 0 s, increases to a new value. (Right) Simultaneous measurement of uncorrected  $45^\circ$  astigmatism.

The RMS wavefront error in astigmatism during the closed loop correction focus was  $341\text{ nm}$ . Since both astigmatism and focus modes are from the same Zernike radial order, they are expected to have the same statistics. Over the first  $12.5$  seconds, when the gain was still set to zero, and assuming a mean offset of  $-426\text{ nm}$ , the RMS focus error is  $265\text{ nm}$ ; the difference due likely to small number statistics of temporally correlated data. Table 2 lists the RMS wavefront error measured as a function of gain value. After the control loop was closed and the gain set to  $0.9$ , the wavefront error in focus drops to  $130\text{ nm}$  RMS, approximately a  $60\%$  reduction compared to the uncompensated astigmatism mode.

Table 2. RMS wavefront error during closed-loop correction of focus as a function of gain factor. \*Focus of zero gain assumes a mean value of  $-426\text{ nm}$ .

Mode	Gain	RMS (nm)	Number of frames
Astigmatism	0	341	12965
Focus	0	265*	1301
	0.2	190	1352
	0.4	127	520
	0.6	142	936
	0.8	144	2600
	0.9	130	6256

Fig. 5 shows the power spectra of the modes shown in Fig. 4 during closed-loop operation. The focus spectrum is split into times of low gain ( $0.2, 0.4$  and  $0.6$ ) and high gain ( $0.8$  and  $0.9$ ). The GLAO loop is correcting for power in

focus below  $\sim 2$  Hz, with greater correction occurring with a higher gain factor. There is a spike in the spectra at 13.7 Hz due to vibrations in the secondary hub.

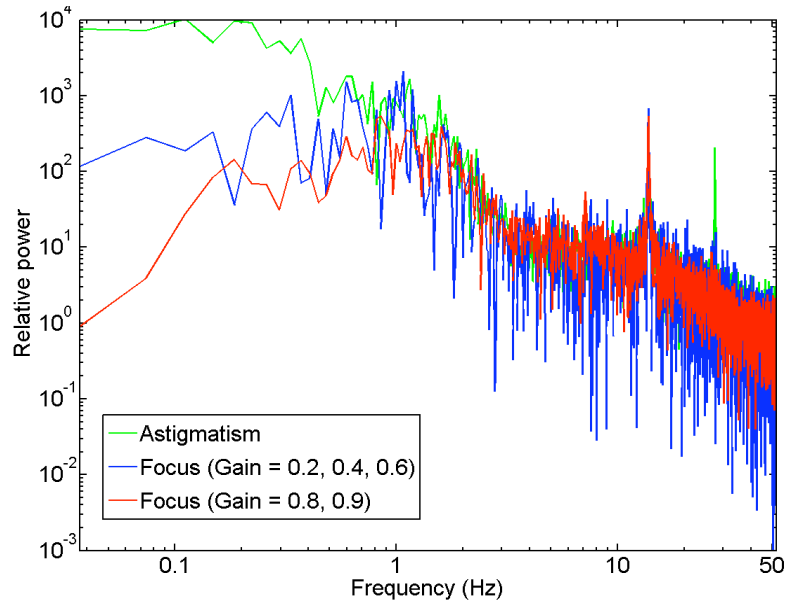


Fig. 5. Power spectrum of astigmatism (green), focus at low gain (0.2, 0.4 and 0.6; blue) and focus at high gain (0.8 and 0.9; red) during closed-loop correction of focus.

The commanded focus position of the ASM has also been recorded. This is shown in Fig. 6 along with the times the gain was changed. The mean position of the mirror during non-zero gain is  $-202$  nm. Because of the factor of two between the mirror shape and the optical path difference added by the mirror, it is compensating for  $-404$  nm of static defocus; agreeing to within 5% with the  $-426$  nm added by the  $20 \mu\text{m}$  hexapod offset.

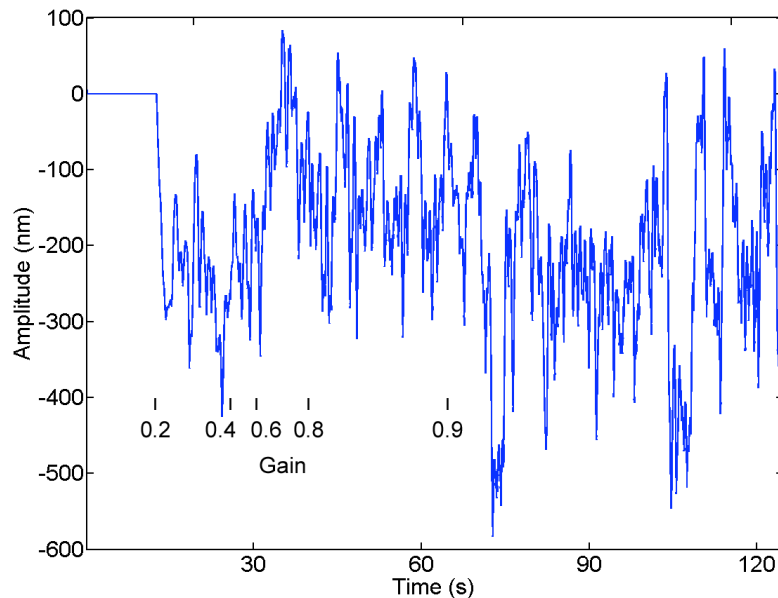


Fig. 6. Adaptive mirror focus mode command during closed-loop correction of focus.

The power spectrum of the commanded focus position of the ASM has also been calculated and appears in Fig. 7. The spectrum has been calculated during times of low and high gain. With a higher gain factor, the adaptive mirror is putting more power into higher frequencies, above  $\sim 1$  Hz, with no noticeable noise floor. However, this does not

lead to a reduction in the power at corresponding frequencies in the residual wavefront error. This is believed to be an artifact of the simple integral controller implemented in the ASM which provides insufficient phase margin at frequencies above a few Hz at the update rate of 208 Hz. In the future this will be addressed by bypassing the ASM's built-in controller and implementing a PID controller on the reconstructor computer, with the addition of a Kalman filter to account for the observed and repeatable noise spikes in the spectra.

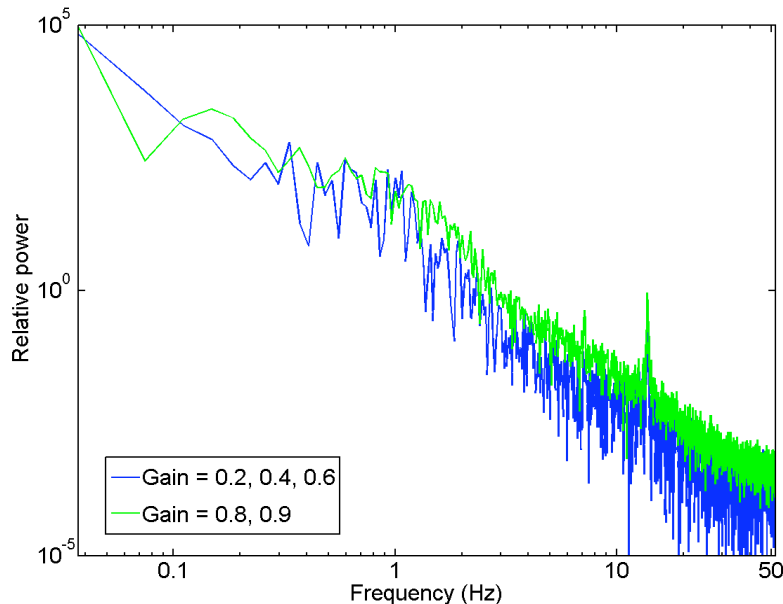


Fig. 7. Power spectra of the adaptive mirror command of focus mode with low gain (blue) and high gain (green) during closed-loop correction of focus.

Following the successful test of focus control, the next step would have been to increase the modal control space one radial order at a time to collect similar data on performance as a function of spatial frequency. This was prevented by very rapid deterioration in weather conditions that rendered the rest of the run unusable.

## 6. CONCLUSIONS

With the very brief sky time available so far, correction of wavefront error with a multi-LGS GLAO approach has been demonstrated for the first time in a limited test. The reduction in power of the focus mode during closed-loop operation shows that the system is functioning and high-order correction is only a few steps away.

Another attempt to commission the system will be made during a telescope run scheduled for October 1 through 4 2007. During this run, it is intended to close the full high-order laser GLAO loop with the tip-tilt loop on a natural guide star. The imaging stability, sensitivity and improvement over a 110 arcsec field will be explored with the near IR imaging camera PISCES which has a plate scale of 0.12 arcsec/pixel, well matched to the expected GLAO PSF. In a subsequent observing run in January 2008, the PSF will be characterized at high resolution using Clio, a thermal infrared camera operating at wavelengths from 1.6 to 4.8  $\mu\text{m}$ , with Nyquist sampling of 0.048 arcsec/pixel. Strehl ratios of 30 to 40% are expected at 4.8  $\mu\text{m}$  in median seeing conditions.

Imaging with both cameras will allow the exploration of parameters which affect GLAO correction. In particular, variables such as control gain, reconstruction basis set and the number of controlled modes need to be optimized. The effect of observing conditions, such as the brightness and field location of the tilt star, also need to be explored so future science programs can anticipate the imaging performance of GLAO correction for particular targets.

Looking forward to future tomographic AO correction at the MMT, detailed calibrations of the optical system will also be made. The ASM will be commanded to assume static shapes and their influence on the measured wavefront of each laser beacon will be recorded. This will map out the pupil from each beacon as it is seen through the Shack-Hartmann prism array and will allow for increased reconstruction fidelity.

Early application to scientific programs will focus on seeing improvement with GLAO, taking advantage of existing near infrared instrumentation [24]. This choice is motivated by a number of considerations. Not only is GLAO the easiest multi-beacon technique to implement, but the MMT's system is likely to remain unique for several years. The exploitation of routine near infrared seeing of 0.2 arcsec or better over a field of several arcminutes is likely to be very productive, both for imaging and high resolution multi-object spectroscopy (MOS) where the many-fold improvement in encircled energy within 0.2 arcsec will be of particular value. In addition, a new high-resolution near-infrared wide field camera, Loki, with both imaging and MOS capabilities, is being designed specifically to take advantage of the wide corrected field afforded by the MMT's ground-layer adaptive optics system [25].

## 7. ACKNOWLEDGEMENTS

Observations reported here were made at the MMT Observatory, a joint facility of The University of Arizona and the Smithsonian Institution. We are grateful for assistance from Matt Rademacher and for the continued support of the MMT Observatory staff. This work has been supported by the Air Force Office of Scientific Research under grant F49620-01-1-0383 and the National Science Foundation under grant AST-0138347.

## 8. REFERENCES

1. Tyler, G. A., Merging: a new method for tomography through random media, *J. Opt. Soc. Am. A* 11, 409–424, 1994.
2. Johns, M., Angel, J. R. P., Shectman, S., Bernstein, R., Fabricant, D., McCarthy, P., and Phillips, M., Status of the Giant Magellan Telescope (GMT) project, in *Ground-Based Telescopes*, J. M. Oschmann, ed., Proc. SPIE 5489, 441–453, 2004.
3. Stepp, L. M. and Strom, S. E., The Thirty-Meter Telescope project design and development phase, in *Second Bäckaskog Workshop on Extremely Large Telescopes*, A. L. Ardeberg & T. Andersen, eds., Proc. SPIE 5382, 67–75, 2004.
4. Andersen, D. et al., Performance modeling of a wide-field ground-layer adaptive optics system, *Publ. Astron. Soc. Pac.* 118, 1574–1590, 2006.
5. Avila, R., Masciadri, E., Vernin, J., and Sánchez, J., Generalized SCIDAR measurements at San Pedro Mártir. I. Turbulence profile statistics, *Publ. Astron. Soc. Pac.* 116, 682–692, 2004.
6. Egner, S., Masciadri, E., McKenna, D., Herbst, T., and Gaessler, W., G-SCIDAR measurements on Mt. Graham—recent results, in *Adaptive Optics II*, B. Ellerbroek & D. Bonaccini Calia, eds., Proc. SPIE 6272, 2006.
7. Lloyd-Hart, M., Baranec, C., Milton, N. M., Stalcup, T., Snyder, M., Putnam, N., and Angel, J. R. P., First tests of wavefront sensing with a constellation of laser guide beacons, *Astrophys. J.* 634, 679–686, 2005.
8. Tokovinin, A. and Travouillon, T., Model of optical turbulence profile at Cerro Pachón, *Mon. Not. R. Astron. Soc.* 365, 1235–1242, 2006.
9. Tokovinin, A., Vernin, J., Ziad, A., and Chun, M., Optical turbulence profiles at Mauna Kea measured by MASS and SCIDAR, *Publ. Astron. Soc. Pac.* 117, 395–400, 2005.
10. Stalcup, T. E., Georges, J. A., Snyder, M., Baranec, C., Putnam, N., Milton, N. M., Angel, J. R. P., and Lloyd-Hart, M., Field tests of wavefront sensing with multiple Rayleigh laser guide stars and dynamic refocus, in *Advancements in Adaptive Optics*, D. Bonaccini, B. L. Ellerbroek, & R. Ragazzoni, eds., Proc. SPIE 5490, 1021–1032 2004.
11. Fugate, R. Q. et al., Measurement of atmospheric wavefront distortion using scattered light from a laser guide-star, *Nature* 353, 141–146, 1991.
12. Brusa, G. et al., MMT adaptive secondary: first AO closed-loop results, in *Astronomical Adaptive Optics Systems and Applications*, eds. R. Tyson & M. Lloyd-Hart, eds., Proc. SPIE 5169, 26–36, 2003.
13. Georges, J., Mallik, P., Stalcup, T., Angel, R., and Sarlot, R., Design and testing of a dynamic refocus system for Rayleigh laser beacons, in *Adaptive Optical System Technologies II*, P. Wizinowich & D. Bonaccini Calia, eds., Proc. SPIE 4839, 473–483, 2002.
14. Rigaut, F., Ground-conjugate wide field adaptive optics for the ELTs, Proc. ESO *Beyond Conventional Adaptive Optics*, E. Vernet, R. Ragazzoni, S. Esposito, & N. Hubin, eds., 58, 11–16, 2002.
15. Le Louarn, M. and Hubin, N., Improving the seeing with wide-field adaptive optics in the near-infrared, *Mon. Not. R. Astron. Soc.* 365, 1324–1332, 2006.
16. Tokovinin, A., Seeing improvement with ground-layer adaptive optics, *Publ. Astron. Soc. Pac.* 116, 941–951, 2004.
17. Marchetti, E. et al., MAD the ESO multi-conjugate adaptive optics demonstrator, in *Adaptive Optical System Technologies II*, P. L. Wizinowich & D. Bonaccini, eds., Proc. SPIE 4839, 317–328, 2003.

18. Stuik, R., Bacon, R., Conzelmann, R., Delabre, B., Fedrigo, E., Hubin, N., Le Louarn, M., and Strobele, S., GALACSI—the ground layer adaptive optics system for MUSE, *New Astron. Rev.* 49, 618–624, 2006.
19. Casali, M. et al., HAWK-I: the new wide-field IR imager for the VLT, in *Ground-based and Airborne Instrumentation for Astronomy*, I. McLean & M. Iye, eds., Proc. SPIE 6269, 2006.
20. Tokovinin, A., Thomas, S., Gregory, B., van der Bliek, N., Schurter, P., Cantarutti, R., and Mondaca, E., Design of ground-layer turbulence compensation with a Rayleigh beacon, in *Advancements in Adaptive Optics*, D. Bonaccini Calia, B. Ellerbroek, & R. Ragazzoni, eds., 5490, 870–878, 2004.
21. Szeto, K. et al., A proposed implementation of a ground layer adaptive optics system on the Gemini Telescope, in *Ground-based and Airborne Instrumentation for Astronomy*, I. McLean & M. Iye, eds., Proc. SPIE 6269, 2006.
22. Lloyd-Hart, M., Angel R., Green, R., Stalcup, T., Milton, N. M., and Powell, K., Multi-laser guide star adaptive optics for the Large Binocular Telescope,” in *Astronomical Adaptive Optics Systems and Applications III*, R. K. Tyson & M. Lloyd-Hart, eds., Proc. SPIE 6691, 2007.
23. Lloyd-Hart, M., Baranec, C., Milton, N. M., Snyder, M., Stalcup, T., and Angel, R., Experimental results of ground-layer and tomographic wavefront reconstruction from multiple laser guide stars, *Opt. Express* 14, 7541–7551, 2006.
24. Lloyd-Hart, M., Stalcup, T., Baranec, C., Milton, N. M., Rademacher, M., Snyder, M., Meyer, M., and Eisenstein, D., Scientific goals for the MMT's multi-laser-guided adaptive optics, in *Advances in Adaptive Optics II*, B. Ellerbroek & D. Bonaccini Calia, eds., Proc. SPIE 6272, 2006.
25. Baranec, C., Lloyd-Hart, M., and Meyer, M., Loki: a ground-layer adaptive optics high-resolution near-infrared survey camera, in *Astronomical Adaptive Optics Systems and Applications III*, R. K. Tyson & M. Lloyd-Hart, eds., Proc. SPIE 6691, 2007.